$Fe^{III}Fe^{III}$ and $Fe^{II}Fe^{III}$ Complexes as Synthetic Analogues for the Oxidized and Reduced Forms of Purple Acid Phosphatases

Ademir Neves* and Marcos A. de Brito

Departamento de Química, Universidade Federal de Santa Catarina, 88040-900, Florianópolis-SC, Brazil

Ivo Vencato and Valderes Drago

Departamento de Física, Universidade Federal de Santa Catarina, 88040-900, Florianópolis-SC, Brazil

Klaus Griesar and Wolfgang Haase

Institut für Physikalische Chemie, Technische Hochschule, Darmstadt, D-6100 Darmstadt, Germany

Received April 14, 1995[⊗]

Novel $Fe^{III}Fe^{III}$ and $Fe^{II}Fe^{III}$ complexes $[Fe_2(BBPMP)(\mu\text{-}OAc)(\mu\text{-}X)]^n$ (**1,** X = OAc^-, $n = 1+$; **2**, X = OH^-, $n = 1+$; **3**, X = OAc^-, $n = 0$; **4**, X = OH^-, $n = 0$), where $BBPMP^{3-}$ is the anion of 2,6-bis[(2-hydroxybenzyl)(2-pyridylmethyl)aminomethyl]-4-methylphenol, and OAc^- is acetate, were prepared in order to provide models for the active site of purple acid phosphatases (PAPs). Complex **1** was obtained by the reaction of H_3BBPMP with $Fe(ClO_4)_2 \cdot 6H_2O$ in methanol and sodium acetate trihydrate under ambient conditions, while complex **3** was synthesized as described for **1,** under an argon atmosphere with low levels of dioxygen. **2** was isolated from **1** in acetonitrile by a substitution of the bridging acetate group by hydroxide, while **4** was generated in solution during a spectropotentiostatic experiment on **2**, under argon. Complex **1**, $[Fe^{III}_2(BBPMP)(\mu\text{-}OAc)_2]ClO_4 \cdot H_2O$, has been characterized by X-ray crystallography. Crystal data: monoclinic, space group $P2_1/n$, $a = 14.863(5)$ Å, $b = 12.315(3)$ Å, $c = 20.872(8)$ Å, $\beta = 90.83(3)°$, $Z = 4$. IR, Mössbauer, magnetic, electronic absorption, and electrochemical properties of **1**−**3** have been investigated, and some of these properties represent a contribution to the understanding of the dinuclear iron center of PAPs. Complexes **2**, $[Fe^{III}_2(BBPMP)(\mu\text{-}OAc)(\mu\text{-}OH)]ClO_4$ ($\lambda_{max} = 568$ nm/$\epsilon = 4760$ M^{-1} cm^{-1}), and **4** $[Fe^{II}Fe^{III}(BBPMP)(\mu\text{-}OAc)(\mu\text{-}OH)]$ ($\lambda_{max} = 516$ nm/$\epsilon = 4560$ M^{-1} cm^{-1}), constitute good synthetic analogues for the chromophoric site for the oxidized and reduced forms, respectively, of the enzyme.

Introduction

Purple acid phosphatases (PAPs) constitute a novel class of metalloenzymes that catalyze the hydrolysis of certain phosphate esters, including nucleoside di- and triphosphates and aryl phosphates, under acidic conditions.[1] Although they have been isolated from a variety of mammalian, plant, and microbial sources, only the enzymes isolated from bovine spleen and porcine uterine fluids (uteroferrin) have been studied in some detail.[1,2] The active site of these PAPs consists of a homonuclear diiron center with two accessible oxidation states: an oxidized $Fe^{III}Fe^{III}$ form (PAPo) and a reduced $Fe^{II}Fe^{III}$ form (PAPr).[3] PAPo is purple, characterized by a typical absorption maximum at 550−570 nm ($\epsilon = 4000$ M^{-1} cm^{-1}), EPR silent, and enzymatically inactive, while PAPr is pink with λ_{max} at 505−515 nm ($\epsilon = 4000$ M^{-1} cm^{-1}) and exhibits acid phophatase activity.[4] These bands are assigned as being tyrosinate-to-iron(III) charge transfer transitions.[4] Resonance Raman spectra of the purple and pink forms, using visible excitation, confirm the presence of tyrosine ring modes.[5] An intense rhombic EPR signal with g values of 1.94, 1.73, and 1.58, observed in PAPr at temperatures less than 30 K, is consistent with an antiferromagnetically coupled high-spin $Fe^{II}Fe^{III}$ ($S = {}^1/_2$) center.[6] Magnetic measurements revealed that the Fe^{II} and Fe^{III} centers are weakly coupled with J values ranging from −5 to −11 cm^{-1}.[5,7] Moreover, a value of $J = -3.0$ cm^{-1} has been established for the reduced phosphate complex on the basis of SQUID magnetization studies.[7]

For the oxidized form, a strong antiferromagnetic coupling ($J > -150$ cm^{-1}) has been estimated from SQUID magnetization measurements.[5] These data suggest that the two Fe(III) atoms should be mediated by a μ-oxo bridge. However, EXAFS[8] and resonance Raman studies[5] do not show any evidence for the existence of such a bridge. In addition, a recent

[⊗] Abstract published in *Advance ACS Abstracts*, March 1, 1996.

(1) (a) Vincent, J. B.; Olivier-Lilley, G. L; Averill, B. A. *Chem. Rev.* **1990,** *90*, 1447. (b) Vincent, J. B.; Averill, B. A. *FASEB J.* **1990,** *4*, 3009. (c) Doi, K.; Antanaitis, B. C.; Aisen, P. *Struct. Bonding (Berlin)* **1988,** *70*, 1. (d) Que, L., Jr.; True, A. E. *Prog. Inorg. Chem.* **1990**, *38*, 97.

(2) (a) Antanaitis, B. C.; Aisen, P. *J. Biol. Chem*. **1984**, *259*, 2066. (b) Antanaitis, B. C.; P. Aisen. *J. Biol. Chem*. **1982**, *257*, 1855. (c) Antanaitis, B. C.; P. Aisen; Lilienthal, H. R. *J. Biol. Chem*. **1983**, *258*, 3166.

(3) (a) Chen, T. T.; Bazer, F. W.; Cetorelli, J. J.; Polland W. E.; Roberts, R. M. *J. Biol. Chem.* **1973**, *258*, 8560. (b) Campbell, H. D.; Dionysius, D. A.; Keough, D. T.; Wilson, B. F.; de Jersey, J.; Zerner, B. *Biochem. Biophys. Res. Commun.* **1978**, *82*, 615.

(4) (a) Antanaitis, B. C.; Aisen, P. *Adv. Inorg. Biochem.* **1983**, *5*, 111. (b) Antanaitis, B. C.; Strekos, T.; Aisen, P. *J. Biol. Chem.* **1982**, *257*, 3766.

(5) Averill, B. A.; Davis, J. C.; Buerman, S.; Zirino, T.; Sanders-Loehr, J.; Loehr, T. M.; Sage, J. T.; Debrunner, P. G. *J. Am. Chem. Soc.* **1987**, *109*, 3760.

(6) Laufer, R. B.; Antanaitis, B. C.; Aisen, P.; Que, L., Jr. *J. Biol. Chem.* **1983**, *258*, 14212.

(7) Day, E. P.; David, S. S.; Peterson, J.; Dunham, W. R.; Bonvoisin, J. J.; Sands, R. H.; Que, L., Jr. *J. Biol. Chem.* **1988**, *263*, 15561.

(8) Kauzlarich, S. M.; Teo, B. K.; Zirino T.; Burman, S.; Davis, J. C.; Averill, B. A. *Inorg. Chem.* **1986**, *25*, 2781.

0020-1669/96/1335-2360$12.00/0

magnetic susceptibility study of PAPo from bovine spleen reveals an antiferromagnetic coupling constant 1 order of magnitude smaller ($J = -15$ cm^{-1}), which indicates the lack of μ-oxo bridge.[9] More recently, on the basis of the pH dependence of activity of the EPR spectra and the visible spectral shifts of the phosphate-saturated PAPr and PAPo from bovine spleen, a dinuclear iron center bridged by carboxylato and hydroxo groups was proposed by Witzel et al.[10]

Mössbauer studies of PAPo from uteroferrin demonstrated the presence of two distinct high-spin Fe(III) centers with strong distortions from octahedral symmetry.[11] The quantitative interconversion of PAPo and PAPr and the similar UV−vis extinction coefficients found for both states indicate that tyrosinate binds only to the iron center that remains trivalent.[1] The presence of histidine as a terminal ligand coordinated at each metal site has been demonstrated by NMR[6,12] and pulsed EPR[13] studies. From the coordination environment proposed for PAPs,[1,6,12] it is clear that the presence of at least one phenolate group as a terminal ligand is required to obtain suitable biomimetic complexes.[14] In fact, a number of dinuclear synthetic analogues of PAPs containing polypodal ligands having pyridine,[15a−d,k] 1-methylimidazole,[15e,f] pyridine−phenolate,[14,15g−i] and 1-methylimidazole−phenolate[15j] as pendant arms have been reported. However, most of these species do not exhibit the characteristic spectral properties found in the purple acid phosphatases. Very recently, we published the synthesis and physicochemical properties of the $[Fe^{III}_2(BBPPNOL)(\mu\text{-}OAc)_2]^+$ complex[16] as a potential model for the visible chromophore of PAPs. The oxidation−reduction chemistry of such complexes with stabilization of the mixed-valence ($Fe^{II}Fe^{III}$) and oxidized (Fe^{III}_2) forms appears to be very informative, since the two forms of PAPs can be interconverted by using oxidants such as ferricyanide and hydrogen peroxide or reductants such as ascorbate and dithioerythrol.[1] Electrochemical studies using coulometric techniques show that the redox potentials for uteroferrin are 0.367 V at pH = 5.0 and 0.306 V at pH = 6.0 vs NHE, which indicates a μ-OH bridging unity.[17]

From the above information one can see that the coordination environment of the dinuclear core of PAPs is not entirely defined, although the presence of some ligands has been unequivocally established. Therefore, the synthesis and characterization of novel dinuclear model complexes with relevant N,O-donor ligands (amine, phenolate, imidazole, and pyridine), capable of stabilizing both Fe^{III}_2 and $Fe^{II}Fe^{III}$, continue being an important area of investigation. In a recent paper, a diphenyl phosphate-bridged analogue of **1** was reported.[15h] In this paper, we report detailed data for two dinuclear iron(III) complexes and their corresponding mixed-valence species with a N_4O_3-donor dinucleating ligand which contains phenolate and pyridine as pendant arms. Some preliminary results of this work have been already presented.[14]

Experimental Section

Abbreviations: H_3BIOMP, 2,6-bis[(((2-hydroxybenzyl)(1-methylimidazol-2-yl)methyl)amino)methyl]-4-methylphenol; HBPMP, 2,6-bis[(bis(2-pyridylmethyl)amino)methyl]-4-methylphenol; H_3BBPPNOL, *N*,*N*′-bis(2-hydroxybenzyl)-*N*,*N*′-bis(2-pyridylmethyl-2-hydroxy-1,3-propanediamine; H_3L, 2,6-bis{[(2-hydroxyphenyl)(2-pyridylmethyl)-amino]methyl}-4-methylphenol; OPr, propionate; OAc, acetate; [TBA]-[PF_6], tetra-*n*-butylammonium hexafluorophosphate.

Materials. Salicylaldehyde, 2-(aminomethyl)pyridine, *p*-cresol, Fe-$(ClO_4)_2$·$6H_2O$, and [TBA][PF_6] were obtained from Aldrich Chemical Co. Thionyl chloride and sodium acetate trihydrate were obtained from Merck. For the electrochemical, spectroelectrochemical, and spectroscopic studies, high-purity solvents were used as received from Merck. High-purity argon was used to deoxygenate the solutions. All other chemicals and solvents were reagent grade.

Syntheses. 2,6-Bis(chloromethyl)-4-methylphenol was prepared as previously described.[15c]

HBPA, (2-Hydroxybenzyl)(2-pyridylmethyl)amine. A mixture of 2-(aminomethyl)pyridine (16.30 g, 151 mmol) and salicylaldehyde (18.56 g, 151 mmol) in 30 mL of methanol was stirred for 15 min at room temperature. After slow addition of $NaBH_4$ (2.0 g, 52.8 mmol) at 0 °C, the solution was concentrated under reduced pressure. The residue was dissolved in 50 mL of water, and the product was extracted with chloroform (6 × 50 mL). The combined organic phases were washed with brine, dried over anydrous $MgSO_4$, which was filtered off, and concentrated under reduced pressure. After a few days at room temperature, X-ray-quality crystals of HBPA were obtained. Yield: 18.5 g; 59%. Mp = 62 °C. Anal. Calcd for $C_{13}H_{14}N_2O$: C, 72.87; H, 6.58; N, 13.07. Found: C, 72.76; H, 5.94; N, 13.01.

H_3BBPMP, 2,6-Bis[((2-hydroxybenzyl)(2-pyridylmethyl)amino)-methyl]-4-methylphenol. A mixture of HBPA (10.0 g, 46.7 mmol) and triethylamine (3.65 g, 36 mmol) in 30 mL of methylene chloride was added dropwise to a THF solution of 2,6-bis(chloromethyl)-4-methylphenol[15c] (4.76 g, 23.2 mmol) under stirring. When the addition was finished, 500 mL of water was added and the residues were filtered off and dissolved in methylene chloride. The resulting solution was washed with brine and dried over anydrous $MgSO_4$, which was filtered off. After concentration of the solution under reduced pressure, the desired ligand (H_3BBPMP), was precipitated with 2-propanol, filtered off, and dried under vacuum. In this way, 8.0 g (50%) of H_3BBPMP was obtained as a white solid. Single crystals suitable for X-ray analysis were obtained by recrystallization from CH_2Cl_2 solution of the ligand. Anal. Calcd for $C_{35}H_{36}N_4O_3$: C, 74.97; H, 6.47; N, 9.99. Found: C, 74.66; H, 6.42; N, 9.87.

$[Fe^{III}_2(BBPMP)(\mu\text{-}OAc)_2]ClO_4$·$H_2O$ (1). To a solution of Fe-$(ClO_4)_2$·$6H_2O$ (1.0 g, 2.75 mmol) in 20 mL of methanol were added sodium acetate trihydrate (0.7 g, 5.1 mmol) and H_3BBPMP (0.60 g, 1.07 mmol). The clear deep blue solution was heated to 40 °C and stirred for 10 min at ambient atmosphere. After cooling of the solution to room temperature, a blue microcrystalline precipitate was formed, which was filtered off and washed with 2-propanol and ether. Yield: 65%. Anal. Calcd for $C_{39}H_{41}N_4O_{12}Fe_2Cl$: C, 51.76; H, 4.56; N, 6.19. Found: C, 51.63; H, 4.56; N, 6.14. Single crystals suitable for X-ray

(9) Gehring, S.; Fleischhauer, P.; Haase, W.; Dietrich, M.; Witzel, H. *Biol. Chem. Hoppe-Seyler* **1990**, *371*, 786.
(10) Dietrich, M.; Münstermann, D.; Suerbaum, H.; Witzel, H. *Eur. J. Biochem.* **1991**, *199*, 105.
(11) De Brunner, P. G.; Hendrich, M. P.; de Jersey, J.; Keough, D. T.; Sage, J. T.; Zerner, B. *Biochim. Biophys. Acta* **1983**, *745*, 103.
(12) Scarrow, R. C.; Pyrz, J. W.; Que, L., Jr. *J. Am. Chem. Soc.* **1990**, *112*, 657.
(13) Antanaitis, B. C.; Peisach, J.; Mims, W. B.; Aisen, P. *J. Biol. Chem.* **1985**, *260*, 4572.
(14) Neves, A.; de Brito, M. A.; Vencato, I.; Drago, V.; Griesar, K.; Haase, W.; Mascarenhas, Y. P. *Inorg. Chim. Acta* **1993**, *214*, 5.
(15) (a) Suzuki, M.; Uehara, A.; Oshio, H.; Endo, K.; Yanaga, M.; Kida, S.; Saito, K. *Bull. Chem. Soc. Jpn.* **1987**, *60*, 3547. (b) Yan, S.; Que, L., Jr.; Taylor, L. F.; Anderson, O. P. *J. Am. Chem. Soc.* **1988**, *110*, 5222. (c) Borovik, A. S.; Papaefthymiou, V.; Taylor, L. F.; Anderson, O. P.; Que, L., Jr. *J. Am. Chem. Soc.* **1989**, *111*, 6183. (d) Maeda, Y.; Tanigawa, Y.; Matsumoto, N.; Oshio, H.; Suzuki, M.; Takashima, Y. *Bull. Chem. Soc. Jpn.* **1994**, *67*, 125. (e) Mashuta, M. S.; Webb, R. J.; Oberhausen, K. J.; Richardson, J. F.; Buchanan, R. M.; Hendrickson, D. N. *J. Am. Chem. Soc.* **1989**, *111*, 2745. (f) Mashuta, M. S.; Webb, R. J.; McCusker, J. K.; Schmitt, E. A.; Oberhausen, K. J.; Richardson, J. F.; Buchanan, R. M.; Hendrickson, D. N. *J. Am. Chem Soc.* **1992**, *114*, 3815. (g) Campbell, V. D.; Parsons, E. J.; Pennington, W. T. *Inorg. Chem.* **1993**, *32*, 1773. (h) Krebs, B.; Schepers, K.; Bremer, B,; Henkel, G.; Althaus, E.; Müller-Warmuth, W.; Griesar, K.; Haase, W. *Inorg. Chem.* **1994**, *33*, 1907. (i) Bernard, E.; Moneta, W.; Laugier, J.; Chardon-Noblat, S.; Deronzier, A.; Tuchagues, J.-P., Latour, J.-M. *Angew. Chem., Int. Ed. Engl.* **1994**, *33*, 887. (j) Nie, H.; Aubin, S. M. J.; Mashuta, M. S.; Wu, C.-C.; Richardson, J. F.; Hendrickson, D. N.; Buchanan, R. M. *Inorg. Chem.* **1995**, *34*, 2382. (k) Shepers, K.; Bremer, B.; Krebs, B.; Henkel, G.; Althaus, E.; Mosel, B.; Müller-Warmurth, W. *Angew. Chem., Int. Ed. Engl.* **1990,** *29*, 531.
(16) Neves, A.; Erthal, S. M. D.; Drago, V.; Griesar, K.; Haase, W. *Inorg. Chim. Acta* **1992**, *197*, 121.
(17) Wang, D. L.; Holz, R. C.; David, S. S.; Que, L., Jr.; Stankovich, M. T. *Biochemistry* **1991**, *30*, 8187.

crystallography were obtained by recrystallization from a 2-propanol−acetone (1:1) solution of **1** (*Caution!* As with all perchlorate salts, samples should be handled with care.)

$[Fe^{III}_2(BBPMP)(\mu\text{-}OAc)(\mu\text{-}OH)]ClO_4\cdot 3H_2O$ (2). To an acetonitrile solution (30 mL) of **1** (0.5 g, 0.5 mmol) were added 5 drops of distilled water and 1 pellet of KOH with magnetic stirring at room temperature. When the solution showed $\lambda_{max} = 532$ nm, the mixture was filtered to remove the excess base and the solution was concentrated under reduced pressure up to dryness. Complex **2** was recrystallyzed from a CH_3CN−hexane mixture (2:1). Yield: 80%. Anal. Calcd for $C_{37}H_{43}N_4O_{13}Fe_2Cl$: C, 49.44; H, 4.82; N, 6.23. Found: C, 49.53; H, 4.31; N, 6.31.

$[Fe^{II}Fe^{III}(BBPMP)(\mu\text{-}OAc)_2]\cdot 4H_2O$ (3). To a solution of $Fe(ClO_4)_2\cdot 6H_2O$ (1.0 g, 2.75 mmol) in methanol (20 mL) were added sodium acetate trihydrate (0.7 g, 5.1 mmol) and H_3BBPMP (0.60 g, 1.07 mmol) under an argon atmosphere with a low level of dioxygen. The mixture was stirred for 60 min. After the deep purple solution was allowed to stand at 10 °C overnight, a microcrystalline precipitate was formed, which was filtered off, and washed with methanol and ether. Yield: 60%. Anal. Calcd for $C_{39}H_{47}N_4O_{112}Fe_2$: C, 54.49; H, 5.51; N, 6.52. Found: C, 53.90; H, 4.93; N, 6.51. Molar conductivity = 66 Ω^{-1} cm^2 M^{-1}.

Physical Methods. Melting points were obtained by using an electrothermal apparatus and are uncorrected. All elemental analyses were performed on a Perkin-Elmer 2400. IR spectra were recorded with a Perkin-Elmer Model 781 spectrometer (Kbr disk), while electronic absorption spectra in the range 180−1800 nm were recorded in CH_3CN with a Perkin-Elmer L19 spectrophotometer. Electrochemical experiments were performed with a Princeton Applied Research (PARC) Model 273 potentiostat/galvanostat, equipped with an IBM/AT-386 microcomputer and an HP-7475 plotter. Cyclic voltammograms (CVs) and differential pulse voltammograms (DPVs) were aquired in acetonitrile containing 0.1 M [TBA][PF_6] as supporting electrolyte, at 100 mV/s, under an argon atmosphere at room temperature. The electrochemical cell employed was of the standard three-electrode configuration: a platinum working electrode, a platinum-wire auxiliary electrode, and an SCE reference electrode constructed in our laboratory. The performance of the reference electrode was monitored by measuring the Fc^+/Fc couple of ferrocene, which was found to have a value of +0.28 V. The half-wave potentials were taken as the average of the anodic and cathodic peak potentials of reversible or quasi-reversible CVs and DPVs. Diagnostic criteria for reversibility of electron-transfer processes were employed in the usual manner.[18] Spectropotentiostatic experiments were performed with the use of an optically transparent thin-layer cell constructed according to a procedure described elsewhere.[19] Potentials were applied to the cell by a potentiostat/galvanostat (PARC 263), and the spectra were collected with a Perkin-Elmer L19 spectrophotometer. The performance of the reference electrode was monitored before and after the experiments, by measuring the Fc^+/Fc couple of ferrocene, which was found to have a value of +0.25 V. Spectral changes were registered after equilibrium was established, following selected potential steps. We allowed 90 s between the recording of each spectrum, and the experiments were stopped when no further changes in the intensity of λ_{max} were observed for the reduced species. Mössbauer spectra were measured at 298 and 115 K against a ^{57}Co (Rh) source moving at constant acceleration. Velocity calibration was carried out by using the resonance lines of metallic iron, and isomer shifts are given relative to iron metal at room temperature. Magnetic susceptibility measurements were performed on polycrystalline samples of the complexes over a temperature range from 4.5 to 296.2 K with a Faraday-type magnetometer; details of the apparatus have been described elsewhere.[20a] Diamagnetic corrections were applied in the usual manner with the use of tabulated Pascal constants.[20b]

X-ray Crystallography. A dark blue prismatic crystal (0.42 × 0.25 × 0.12 mm) of $[Fe^{III}_2(BBPMP)(\mu\text{-}OAc)_2]ClO_4\cdot H_2O$ was mounted on a CAD-4 Enraf-Nonius diffractometer. The cell parameters were obtained by a least-squares fit of 25 reflections ($16.0° < \theta < 30.0°$). Crystal parameters are given in Table 1. The intensity data were collected by using an $\omega-2\theta$ scan mode, graphite-monochromated Cu Kα radiation (1.540 562 Å), a scan speed of 4−20°/min, and a scan range of $(0.80 + 0.35 \tan\theta)°$. No significant decline in intensities of two standard reflections was observed. The data were corrected for Lorentz and polarization effects. The number of measured reflections was 5297 in the range −15/15, 0/10, 0/22 with 4393 unique reflections and 1856 with $I > 3\sigma(I)$. The systematic absences were $h0l$, $h + k \neq 2n$, and $0kl$, $k \neq 2n$, consistent with the space group $P2_1/n$ (C_{2h}^5; No. 14). Equivalent reflections were merged with $R_{int} = 4.81\%$. The structure was solved using SHELX86[21a] and successive Fourier syntheses. The structure was refined by a least-squares procedure that utilized a "blocked-cascade" algorithm. The function minimized during the least-squares refinement was $\sum w(|F_o| - |F_c|)^2$ where $w = k|\sigma^2(F_o) + gF_o^2|^{-1}$, with $k = 2.0506$, $g = 0.002\,500$, and $\sigma(F_o)$ = the esd for the observed amplitudes based on counting statistics. The positions of H atoms were calculated and included in the final refinement cycle using the SHELX-76[21b] program. An empirical absorption correction (DIFABS) was applied, with maximum and minimum transmission factors of 1.619 and 0.651. All non-hydrogen atoms were refined with the use of anisotropic thermal parameters. The number of refined parameters was 510. In the final refinement cycle ($R = 0.0752$ and $R_w = 0.0784$) a maximum $\Delta/\sigma = 0.41$ and a maximum height in the final ΔF map of 0.72 e Å^{-3} were observed. During all calculations, the analytical scattering factors for neutral atoms were corrected for both $\Delta f'$ and $i(\Delta f'')$ terms. The calculations were carried out on an IBM/3090 computer using the SHELX-76 program package and the scattering factors taken from ref 21c.

Table 1. Crystallographic Parameters for $[Fe^{III}_2(BBPMP)(\mu\text{-}OAc)_2]ClO_4\cdot H_2O$

chem formula	$C_{39}H_{41}N_4O_{12}Fe_2Cl$	Z	4
fw	904.92	T, °C	25
space group	$P2_1/n$ (No. 14)	λ, Å	1.540 562
a, Å	14.863(5)	ρ_{calc}, g cm^{-3}	1.65
b, Å	12.315(3)	μ, cm^{-1}	21.3
c, Å	20.872(8)	R,[a] %	7.52
β, deg	90.83(3)	R_w,[b] %	7.84
V, Å^3	3820.0		

[a] $R = \sum||k|F_o| - |F_c||/\sum k|F_o|$. [b] $R_w = [\sum w(k|F_o| - |F_c|)^2/\sum wk^2F_o^2]^{1/2}$; $w = k[\sigma^2(|F_o| + g|F_o|^2)]^{-1}$; $k = 2.0506$; $g = 0.002\,500$.

Results and Discussion

Syntheses. A dinuclear iron center with two accessible oxidation states, $Fe^{III}Fe^{III}$ and $Fe^{II}Fe^{III}$, has been well established for the active site of PAPs isolated from bovine spleen and porcine uterus.[2] In an attempt to gain more information concerning the coordination environment of the iron centers in these metalloproteins, we[14,16] and Krebs's group[15h] are currently investigating the syntheses and characterization of new iron complexes with N,O-donor dinucleating ligands having terminal phenolate and pyridine binding groups. The ligand H_3BBPMP is produced in good yield by nucleophilic substitution of 2,6-bis(chloromethyl)-4-methylphenol with HBPA in THF solution containing Et_3N. This ligand reacts in methanol with 2 equiv of $Fe(ClO_4)_2\cdot 6H_2O$ in the presence of sodium acetate trihydrate at ambient atmosphere to form the dark-blue and stable complex $[Fe^{III}_2(BBPMP)(\mu\text{-}OAc)_2]ClO_4\cdot H_2O$ (**1**). Complex **2** was synthesized from **1** in CH_3CN/H_2O/KOH via a reaction substituting one bridging acetate group by one μ-OH. The synthesis was monitored by visible absorption spectroscopy and the reaction was stopped when the basic acetonitrile solution of **2** showed $\lambda_{max} = 532$ nm. Below this point, the complex appears to

(18) Nicholson, R. S.; Shain, I. *Anal. Chem.* **1964**, *36*, 706.
(19) Neves, A.; Erthal, S. M. D.; Vencato, I.; Ceccato, A. S.; Mascarenhas, Y. P.; Nascimento, O. R.; Hörner, M.; Batista, A. A. *Inorg. Chem.* **1992**, *31*, 4749.
(20) (a) Merz, L.; Haase, W. *J. Chem. Soc., Dalton Trans.* **1980**, 875. (b) O'Connor, C. J. *Prog. Inorg. Chem.* **1982**, *29*, 203.
(21) (a) Sheldrick, G. M. *SHELXS86:* Program for the Solution of Crystal Structures. University of Göttingen, Germany, 1986. (b) Sheldrick, G. M. SHELX-76: Program for Crystal Structure Determination. University of Cambridge, England, 1986. (c) *International Tables for X-Ray Crystallography*; Kynoch Press: Birmingham, U.K., 1974; Vol. IV.

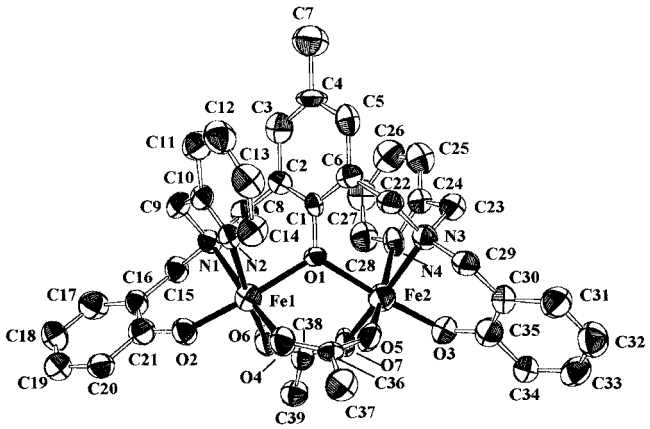

Figure 1. Structure of the cations of **1**, showing the atom-labeling scheme.

dissociate, and we were not able to isolate the corresponding $(\mu\text{-OH})_2$ analogue of **2**. The synthesis of the mixed-valence $[Fe^{II}Fe^{III}(BBPMP)(\mu\text{-OAc})_2]$ complex, **3**, was achieved by treating a methanolic solution of H_3BBPMP with 2 equiv of $Fe(ClO_4)_2\cdot 6H_2O$ and 2 equiv of sodium acetate trihydrate under an argon atmosphere with low levels of dioxygen. This purple $Fe^{II}Fe^{III}$ complex is very stable in the solid state, even in the presence of air, but oxidizes in solution under aerobic conditions. Complexes **1**−**3** exhibit one symmetrical $\nu_{sym} = 1450\ cm^{-1}$ and one asymmetrical $\nu_{asym} = 1570\ cm^{-1}$ stretching mode for the acetate bridging groups, which suggests the same mode of coordination of the ligand in the complexes.[16] Stretching vibrations of the uncoordinated ClO_4^- are located at 1100 and 1090 cm^{-1} for complexes **1** and **2,** respectively, and are absent for $[Fe^{II}Fe^{III}(BBPMP)(\mu\text{-OAc})_2]$, confirming the neutral character of this complex according to the molar conductivity experiment (66 $\Omega^{-1}\ cm^2\ M^{-1}$).[22] In addition, the Mössbauer, magnetic susceptibility, and electrochemmical data, together with elemental analyses and electronic spectroscopy, support the formulation for complexes **2** and **3**, when compared to **1**.

Crystal and Molecular Structure of $[Fe^{III}_2(BBPMP)(\mu\text{-OAc})_2]ClO_4\cdot H_2O$ (1). The structure of complex **1** consists of discrete dimeric $[Fe^{III}_2(BBPMP)(\mu\text{-OAc})_2]^+$ cations, uncoordinated perchlorate anions, and a water of crystallization in the crystallographic asymmetric unit. An ORTEP drawing of the complex cation with its atom-labeling scheme is shown in Figure 1. The atomic parameters and selected bond distances and angles are given in Tables 2 and 3 respectively. No crystallographic symmetry is imposed on the cation, resulting in the observation of distinct ferric sites in the complex. The metal centers are bridged by the phenolate oxygen atom of the $BBPMP^{3-}$ dinucleating ligand and by two acetate ligands. The nitrogen (amine and pyridyl) and oxygen (phenolate) donors of the ligand complete the octahedral environment of the two iron centers in a facial terminal arrangement. A similar arrangement around the iron(III) centers has been detected in the related $[Fe^{III}_2(BIOMP)(\mu\text{-OAc})_2]ClO_4\cdot H_2O$ complex,[15j] in which the H_3BIOMP ligand contains 1-methylimidazole instead of pyridine groups. Interestingly, the two terminal phenolate oxygen donor atoms coordinate *trans* to the bridging phenolate group in both complexes. This result constrasts with that observed in the closely related $[LCo_2^{III}(\mu\text{-OPr})_2]^+$ complex[15g] with a similar N,O-donor set, in which two pyridyl groups are *trans* rather than *cis* to the bridging phenolate. The distinct coordination arrangements observed in the structures probably arise from the different N(amine)⌒&⌒O(phenolate) chelate rings present in these complexes (six-membered in $[Fe^{III}_2(BBPMP)(\mu\text{-OAc})_2]ClO_4\cdot H_2O$ and $[Fe^{III}_2(BIOMP)(\mu\text{-OAc})_2]ClO_4\cdot H_2O$ and five-membered in $[L\ Co^{III}_2(\mu\text{-OPr})_2]^+$). Unfortunately, a full crystal structure description for $[LFe^{III}_2(\mu\text{-OPr})_2]^+$ [15g] is not yet available for further comparisons. Recently, Krebs et al.[15h] reported a diphenyl phosphate-bridged analogue of **1** with the same mode of coordination of the ligand around the iron centers but with remarkable differences in bond angles and distances.

Table 2. Atomic Parameters for $[Fe^{III}_2(BBPMP)(\mu\text{-OAC})_2]ClO_4\cdot H_2O$

atom	*x*	*y*	*z*	B_{eq},[a] Å^2
Fe(1)	0.3529(2)	0.3750(2)	0.2975(1)	4.09(8)
Fe(2)	0.5268(2)	0.4103(2)	0.1861(1)	4.18(8)
O(1)	0.4821(5)	0.3422(6)	0.2697(3)	2.7(2)
O(2)	0.2392(6)	0.4046(7)	0.3280(4)	3.7(2)
O(3)	0.5720(5)	0.4611(7)	0.1090(3)	3.7(2)
O(4)	0.3057(6)	0.3343(7)	0.2124(4)	4.2(2)
O(5)	0.4162(6)	0.3493(7)	0.1447(3)	4.0(2)
O(6)	0.3749(6)	0.5305(7)	0.2795(4)	4.3(2)
O(7)	0.4781(6)	0.5523(7)	0.2092(4)	4.2(2)
N(1)	0.4047(7)	0.3878(8)	0.3954(4)	3.1(2)
N(2)	0.3491(7)	0.2093(8)	0.3272(5)	3.5(2)
N(3)	0.5964(7)	0.2584(8)	0.1692(4)	3.3(2)
N(4)	0.6501(7)	0.4338(8)	0.2372(5)	3.5(2)
C(1)	0.5359(8)	0.281(1)	0.3069(6)	2.6(2)
C(2)	0.5470(9)	0.306(1)	0.3691(6)	3.7(2)
C(3)	0.603(1)	0.236(1)	0.4074(6)	4.5(2)
C(4)	0.6423(9)	0.148(1)	0.3809(7)	4.2(2)
C(5)	0.6305(9)	0.124(1)	0.3176(7)	3.9(2)
C(6)	0.5765(9)	0.194(1)	0.2789(6)	3.3(2)
C(7)	0.700(1)	0.077(1)	0.4211(8)	6.4(2)
C(8)	0.5022(9)	0.399(1)	0.3993(6)	3.7(2)
C(9)	0.3768(9)	0.283(1)	0.4292(6)	4.1(2)
C(10)	0.3711(8)	0.191(1)	0.3859(6)	3.1(2)
C(11)	0.396(1)	0.088(1)	0.4092(7)	4.6(2)
C(12)	0.388(1)	0.002(1)	0.3685(7)	5.1(2)
C(13)	0.360(1)	0.020(1)	0.3067(7)	4.5(2)
C(14)	0.3415(9)	0.124(1)	0.2864(6)	4.3(2)
C(15)	0.3644(9)	0.487(1)	0.4267(6)	3.7(2)
C(16)	0.2638(9)	0.490(1)	0.4281(6)	3.4(2)
C(17)	0.227(1)	0.540(1)	0.4815(7)	5.0(2)
C(18)	0.136(1)	0.552(1)	0.4869(7)	5.1(2)
C(19)	0.082(1)	0.518(1)	0.4390(7)	4.6(2)
C(20)	0.1158(9)	0.469(1)	0.3859(6)	3.8(2)
C(21)	0.2091(9)	0.453(1)	0.3805(6)	4.0(2)
C(22)	0.5650(9)	0.169(1)	0.2105(6)	3.4(2)
C(23)	0.6943(9)	0.280(1)	0.1797(6)	4.0(2)
C(24)	0.7098(9)	0.354(1)	0.2344(6)	3.7(2)
C(25)	0.780(1)	0.339(1)	0.2752(7)	5.2(2)
C(26)	0.789(1)	0.410(1)	0.3275(8)	6.1(2)
C(27)	0.728(1)	0.490(1)	0.3331(7)	4.8(2)
C(28)	0.660(1)	0.502(1)	0.2888(7)	5.1(2)
C(29)	0.5796(9)	0.224(1)	0.1008(6)	3.5(2)
C(30)	0.6061(8)	0.302(1)	0.0513(6)	3.5(2)
C(31)	0.634(1)	0.256(1)	−0.0053(7)	5.0(2)
C(32)	0.650(1)	0.320(1)	−0.0579(7)	5.7(2)
C(33)	0.640(1)	0.432(1)	−0.0520(7)	4.8(2)
C(34)	0.6113(9)	0.480(1)	0.0022(6)	3.9(2)
C(35)	0.5949(9)	0.412(1)	0.0566(6)	4.4(2)
C(36)	0.3380(8)	0.322(1)	0.1582(5)	2.4(2)
C(37)	0.280(1)	0.279(1)	0.1087(7)	4.5(2)
C(38)	0.4197(9)	0.589(1)	0.2435(6)	3.7(2)
C(39)	0.4005(9)	0.707(1)	0.2420(6)	4.3(2)
Ow	−0.066(1)	0.220(1)	0.3944(7)	12.6(2)
Cl	0.5640(3)	0.7443(4)	0.3963(2)	7.0(1)
O(8)	0.578(1)	0.750(1)	0.3303(8)	9.7(2)[b]
O(9)	0.602(2)	0.828(2)	0.423(1)	14.6(2)[b]
O(10)	0.479(1)	0.740(2)	0.4124(9)	12.8(2)[b]
O(11)	0.603(1)	0.647(1)	0.4202(8)	11.3(2)[b]
O(8)′	0.576(2)	0.837(3)	0.341(2)	4.2(2)[c]
O(9)′	0.657(2)	0.719(2)	0.419(2)	2.5(2)[c]
O(10)′	0.520(2)	0.821(2)	0.442(1)	1.2(2)[c]
O(11)′	0.492(3)	0.672(3)	0.377(2)	8.9(2)[c]

[a] $B_{eq} = {}^4/_3\sum_{ij}\beta_{ij}(\mathbf{a}_i\cdot\mathbf{a}_j)$. [b] Occupancy factor 0.799. [c] Occupancy factor 0.201.

(22) Geary, W. J. *Coord. Chem. Rev.* **1971**, *7*, 81.

Table 3. Selected Bond Distances (Å) and Angles (deg) for $[Fe^{III}_2(BBPMP)(\mu\text{-}OAc)_2]ClO_4\cdot H_2O$

	Bond Distances		
Fe(1)−O(1)	2.054(8)	Cl−O(8)	1.40(2)
Fe(1)−O(2)	1.851(9)	Cl−O(9)	1.30(2)
Fe(1)−O(4)	1.965(8)	Cl−O(10)	1.31(2)
Fe(1)−O(6)	1.980(9)	Cl−O(11)	1.42(2)
Fe(1)−N(1)	2.18(1)	Cl−O(8)′	1.64(3)
Fe(1)−N(2)	2.13(1)	Cl−O(9)′	1.49(3)
Fe(2)−O(1)	2.055(7)	Cl−O(10)′	1.50(3)
Fe(2)−O(3)	1.861(8)	Cl−O(11)′	1.44(4)
Fe(2)−O(5)	1.993(9)		
Fe(2)−O(7)	1.956(9)		
Fe(2)−N(3)	2.17(1)		
Fe(2)−N(4)	2.13(1)		
Fe(1)···Fe(2)	3.528(8)		
	Bond Angles		
O(1)−Fe(1)−O(2)	176.3(3)	O(1)−Fe(1)−N(2)	85.6(3)
O(1)−Fe(1)−O(4)	91.0(3)	O(2)−Fe(1)−O(4)	92.6(4)
		O(2)−Fe(1)−O(6)	91.7(4)
O(1)−Fe(1)−O(6)	88.8(3)	O(2)−Fe(1)−N(1)	88.6(4)
O(1)−Fe(1)−N(1)	87.7(3)	O(2)−Fe(1)−N(2)	93.5(4)
O(4)−Fe(1)−O(6)	97.6(4)	O(3)−Fe(2)−N(3)	88.3(4)
O(4)−Fe(1)−N(1)	169.3(4)	O(3)−Fe(2)−N(4)	93.9(4)
O(4)−Fe(1)−N(2)	90.5(4)	O(5)−Fe(2)−O(7)	97.9(3)
O(6)−Fe(1)−N(1)	92.9(4)	O(5)−Fe(2)−N(3)	89.8(4)
O(6)−Fe(1)−N(2)	170.2(4)	O(5)−Fe(2)−N(4)	165.5(4)
N(1)−Fe(1)−N(2)	78.9(4)	O(7)−Fe(2)−N(4)	94.2(4)
		O(7)−Fe(2)−N(3)	172.1(4)
O(1)−Fe(2)−O(3)	175.3(3)	N(3)−Fe(2)−N(4)	77.8(4)
O(1)−Fe(2)−O(5)	86.5(3)	Fe(1)−O(1)−Fe(2)	118.3(4)
O(1)−Fe(2)−O(7)	91.7(3)	Fe(1)−O(4)−O(5)	107.5(4)
O(1)−Fe(2)−N(3)	87.0(3)	Fe(2)−O(5)−O(4)	111.9(4)
O(1)−Fe(2)−N(4)	85.2(3)	Fe(1)−O(6)−O(7)	111.8(5)
O(3)−Fe(2)−O(5)	93.3(4)	Fe(2)−O(7)−O(6)	109.0(4)
O(3)−Fe(2)−O(7)	93.0(4)	O(8)′−Cl−O(9)′	105(1)
O(8)−Cl−O(9)	108(1)	O(8)′−Cl−O(10)′	94(1)
O(8)−Cl−O(10)	114(1)	O(8)′−Cl−O(11)′	109(1)
O(8)−Cl−O(11)	109(1)	O(9)′−Cl−O(10)′	110(1)
O(9)−Cl−O(10)	110(1)	O(9)′−Cl−O(11)′	130(1)
O(9)−Cl−O(11)	110(1)	O(10)′−Cl−O(11)′	104(1)
O(10)−Cl−O(11)	105(1)		

Undoubtedly, these changes can be correlated with the rigid character of diphenyl phosphate when compared to the acetate group.

In the dinuclear cation of **1**, each of the iron centers has a tertiary amine nitrogen atom and one pyridyl group, which coordinate *trans* to the oxygen atoms of the carboxylato bridges. The five-membered chelate rings formed by the N(amine) and N(pyridyl) donors at each of the iron centers are rotated by ≈180° with respect to each other and the carboxylato groups, which are also related by the same pseudo-2-fold axis, so that the carboxylato groups are coordinated in an asymmetric fashion. The Fe(III)−O(carboxylato) bond lengths [average 1.960(8) Å] *trans* to the tertiary amine atoms are somewhat shorter than the Fe(III)−O(carboxylato) lengths [average 1.978(8) Å] *trans* to the pyridyl nitrogen donors. This can be associated with the Fe(III)−N(amine) distances [average 2.175(10) Å], which are larger than the Fe(III)−N(pyridyl) bonds [average 2.130(10) Å]. Similar structural observations have been reported for $[Fe^{III}_2(BIOMP)(\mu\text{-}OAc)_2]^{+}$ [15j] and for the mixed-valence $[Fe_2(BPMP)(\mu\text{-}OPr)_2]^{2+}$ [15c] complex and can be explained in terms of the constraining nature of these ligands. As with the $[Fe^{II}Fe^{III}(BPMP)(\mu\text{-}OPr)_2]^{2+}$ [15c] and $[Fe^{III}_2(BBPMP)(\mu\text{-}O_2P(OPh)_2)_2]^{+}$,[15h] the $N_{amine}-Fe-N_{pyridyl}$ chelate angles in complex **1** are significantly less than 90° [N(1)−Fe(1)−N(2) = 78.9(4)° and N(3)−Fe(2)−N(4) = 77.9(4)°], confirming the ring strain caused by the pyridyl arms. The Fe(III)−O bond lengths with the bridging phenolate group [Fe(1)−O(1) = 2.054(8) and Fe(2)−O(1) = 2.056(8) Å] in **1** are significantly longer than the corresponding Fe(III)−O(phenolate) bond distance observed in the $[Fe^{II}Fe^{III}(BPMP)(\mu\text{-}OPr)_2]^{2+}$ complex (1.943(2) Å).[15c] This is a reflection of the short terminal Fe(III)−O(phenolate) bond lengths (Fe(1)−O(2) = 1.850(8) and Fe(2)−O(3) = 1.861(8) Å) which are coordinated in *trans* positions to the bridged phenolate group in **1**. Furthermore, one can note that the Fe(1)−O(1)−Fe(2) bridging angle of 118.3(4)° in **1** is somewhat larger than the 113.1(1)° value observed for the $[Fe^{II}Fe^{III}(BPMP)(\mu\text{-}OPr)_2]^{2+}$ complex but is shorter than the 128.2(4)° value for $[Fe^{III}_2(BBPMP)(\mu\text{-}O_2P(OPh)_2)_2]^{+}$.[15h] Consequently, the Fe···Fe distance of 3.528(8) Å for **1** is larger than the analogous distance in the $BPMP^{-}$ complex (3.365(1) Å) and shorter than that in the $(\mu\text{-}O_2P(OPh)_2)_2$ complex (3.837(8) Å).[15h]

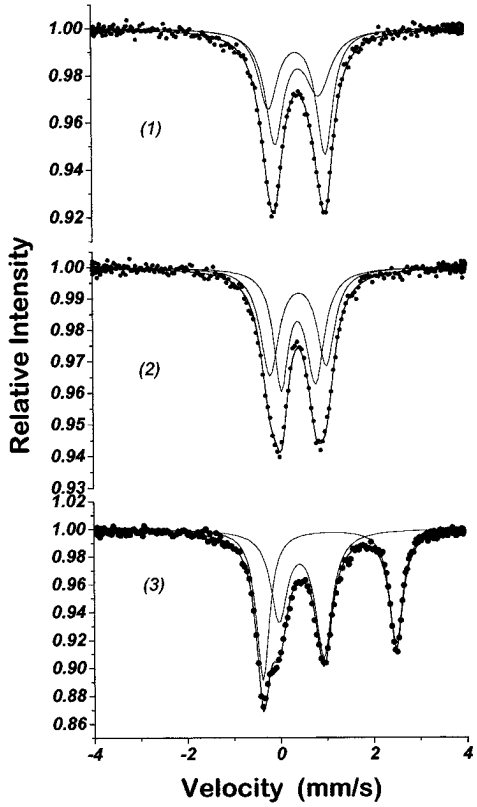

Figure 2. Mössbauer spectra of polycrystalline samples of **1** (top), **2**, and **3** (bottom) at 115 K.

Finally, atoms O(8)···O(11) were found to be disordered beween two positions. This disorder was modeled by the addition of four new atomic positions, O(8)′···O(11)′, and refined isotropically. The site occupation factors of the original atomic positions were then refined as one number, 0.799(2), and the complement of the refined site occupation factor was used as the site occupation factor of the new atomic positions.

Mössbauer Spectroscopy. Mössbauer spectroscopy was used to assign the oxidation states of the iron centers in these dinuclear complexes. Representative spectra of complexes **1**−**3** at 115 K are given in Figure 2, and the Mössbauer parameters are listed in Table 4. The parameters observed for complexes **1** and **2** are typical of high-spin Fe(III) ions,[23] in agreement with the magnetic susceptibility data, and are comparable to those detected for the oxidized form of $(PAP)PO_4$[5] and the analogues model complexes listed in Table 4. These obsevations, together with the X-ray crystal structure of **1** (Figure 1), clearly show that the Mössbauer spectra are not affected by the small diferences in the coordination environments of the two iron sites in **1** and **2**.

For the mixed-valence $Fe^{II}Fe^{III}$ complex **3** two doublets (four Lorentzians of equal areas) were used to fit the spectra. The

(23) Greenwood, N. N.; Gibb, T. C. *Mössbauer Spectroscopy;* Chapman and Hall: London, 1971; pp 113−168.

Table 4. Mössbauer Parameters of the Complexes

	T, K	δ, mm/s	ΔE_q, mm/s	Γ, mm/s	% area of absorption	ref
$[Fe^{III}_2(BBPMP)(\mu\text{-}OAc)_2]ClO_4$	298	0.41	1.06	0.65	100	
	115	0.46	1.09	0.53	100	this work
$[Fe^{III}_2(BBPMP)(\mu\text{-}OAc)(\mu\text{-}OH)]ClO_4$	298	0.40	0.96	0.59	100	
	115	0.50	0.97	0.57	100	this work
$[Fe^{II/III}_2(BBPMP)(\mu\text{-}OAc)_2]$	298	0.41	1.08	0.31	50	
		1.06	2.81	0.29	50	
	115	0.53	0.96	0.43	50	
		1.13	2.86	0.35	50	this work
$[Fe^{III}_2(BBPMP)(\mu\text{-}O_2P(OPh)_2)_2]ClO_4$	300	0.36		0.82	100	
	70	0.48		1.24	100	15h
$[Fe^{III}_2(L)(\mu\text{-}OPr)_2]BF_4$	298	0.37	0.77		100	15g
$[Fe^{III}_2(BIOMP)(\mu\text{-}OAc)_2]ClO_4$	295	0.41	1.08			
	125	0.51	1.06			15j
$[Fe^{III}_2(BBPPNOL)(\mu\text{-}OAc)_2]PF_6$	300	0.39	1.22	0.59	50	
		0.41	1.00	0.59	50	
	115	0.50	1.27	0.40	50	
		0.50	0.89	0.40	50	16
$[Fe^{III}_2(BBPPNOL)(\mu\text{-}O_2P(OPh)_2)_2]BPh_4$	300	0.40	0.66	0.43		
		0.40	1.22	0.40		
	50	0.52	0.65	0.36		15h
$[Fe^{II}Fe^{III}(BPMP)(\mu\text{-}OAc)_2](BF_4)_2$	77	1.16	2.42	0.41	49	
		0.47	0.51	0.33	51	15a
$[Fe^{II}Fe^{III}(BPMP)(\mu\text{-}OPr)_2](BPh_4)_2$	300	0.96	1.83	0.38	51	
		0.41	0.53	0.28	49	15c
purple bovine spleen PO_4	100	0.47	0.99			
		0.53	1.32			5
pink uteroferrin	100	0.52	1.83			
		1.22	2.66			11

Table 5. *J* Values of the Dinuclear Complexes

complex	J, cm^{-1}	ref
$[Fe^{II/III}_2(BPMP)(\mu\text{-}OAc)_2](BF_4)_2\cdot H_2O$	−3.2	15a
$[Fe^{II/III}_2(BBPMP)(\mu\text{-}OAc)_2]\cdot H_2O$	−5.3	this work
$[Fe^{III}_2(BBPMP)(\mu\text{-}O_2P(OPh)_2)_2]ClO_4\cdot H_2O$	−5.7	15h
$[Fe^{III}_2(BBPMP)(\mu\text{-}OAc)_2]ClO_4\cdot H_2O$	−6.0	this work
$[Fe^{III}_2(BIOMP)(\mu\text{-}OAc)_2]ClO_4\cdot H_2O$	−6.4	15j
$[Fe^{III}_2(BBPMP)(\mu\text{-}OAc)(\mu\text{-}OH)]ClO_4\cdot 3H_2O$	−10.6	this work
$[Fe^{III}_2(BBPPNOL)(\mu\text{-}OAc)_2]ClO_4$	−13.7	16
$Fe^{II}Fe^{III}$ bovine spleen	−11.0(3)	9
$Fe^{III}Fe^{III}$ bovine spleen	−15.0	9

isomer shift, δ, values of 0.53 and 1.13 mm/s and the quadrupole splitting, ΔE_Q, values of 0.96 and 2.86 mm/s at 115 K are assigned to a high-spin Fe^{III} center and a high-spin Fe^{II} center, respectively,[23] in agreement with the magnetic susceptibility data. These parameters, with exception of the ΔE_Q value of 0.96 mm/s attributed to the Fe^{III} center, fall in the range observed for most of the mixed-valence $Fe^{II}Fe^{III}$ complexes described in the literature. [15a,c] The large ΔE_Q value for the Fe^{III} center probably is a reflection of major distortions from effective octahedral symmetry as has been observed in the X-ray crystal structure of complex **1**, which shows similar Mössbauer parameters for the iron(III) center. From this information it seems reasonable to assume that the one-electron reduction of **1** does not cause significant change in the electronic charge distribution at the iron center that remains oxidized. Indeed, this interpretation is well corroborated by the fact that the mixed-valence complex **3** is valence-trapped in the solid state, even at room temperature, as indicated by the observation of discrete quadrupole doublets (Figure 2). These results strongly suggest that, in the solid state, complexes **1**−**3** probably have similar coordination environments. Furthermore, it is worthy of note that the Mössbauer parameters for complex **3** are comparable to those reported for PAPr[11] (Table 4). This fact reflects, at least to some extent, structural similarities between the distorted octahedral coordination environment of the iron(III) centers in the present complexes (N_2O_4 site) and that proposed for the nonreducible iron center in the protein (NO_5 site).[1]

Magnetic Susceptibility Measurements. The variable-temperature magnetic data for complexes **1**−**3** in the solid state, collected in the temperature range 4.5−296.2 K, are shown in Figure 3 and indicate the presence of weak antiferromagnetic coupling processes. The data were fitted by using the expression for molar susceptibility versus temperature from the spin-exchange Hamiltonian $H = -2JS_1S_2$ ($S_1 = S_2 = {}^5/_2$, for **1** and **2**, and $S_1 = 2$, $S_2 = {}^5/_2$ for **3**), and the following parameters: $g = 2.00$ (fixed), $D = 0.0$ cm^{-1} and TIP = 400×10^{-6} cm^3/mol for **1**−**3**; $J = -6.0$ (± 1) cm^{-1}, % impurity = 1.7 (± 0.1) for **1**; $J = -10.6$ (± 1) cm^{-1}, % impurity = 2.4 for **2**; $J = -5.3(\pm 1)$ cm^{-1}, % impurity = 2.5 for **3**. A J value of $-6.0(\pm 1)$ cm^{-1} for $[Fe^{III}_2(BBPMP)(\mu\text{-}OAc)_2]ClO_4$ is in good agreement with $J = -5.7(\pm 1)$ cm^{-1} and $J = -6.4$ cm^{-1} found for $[Fe^{III}_2(BBPMP)(\mu\text{-}O_2P(OPh)_2)_2]ClO_4$[15h] and $[Fe^{III}_2(BIOMP)(\mu\text{-}OAc)_2]ClO_4\cdot H_2O$,[15j] respectively. On the other hand, the J value of -10.6 cm^{-1} for $[Fe^{III}_2(BBPMP)(\mu\text{-}OAc)(\mu\text{-}OH)]ClO_4$, when compared to **1** and $[Fe^{III}_2(BIOMP)(\mu\text{-}OAc)_2]ClO_4\cdot H_2O$ suggests an improvement of $\cong -5.0$ cm^{-1} for a substitution of one acetate bridging group by a μ-OH and leads us to speculate about a mixed (μ-OAc/μ-OH) bridging unity, according to Witzel et al.,[10] for the active center of PAPo. The J value of 15.0 cm^{-1} determined by Haase et al.[9] for the purple form of bovine spleen strongly corroborates this trend. A J value of $-5.3(\pm 1)$ cm^{-1} for $[Fe^{II}Fe^{III}(BBPMP)(\mu\text{-}OAc)_2]$ is somewhat similar to the J value of -3.2 cm^{-1} for $[Fe^{II}Fe^{III}(BPMP)(\mu\text{-}OAc)_2](BF_4)_2$,[15a] and these observations are in agreement with a weak antiferromagnetic coupling process for the pink form of PAPs.[5,7]

Electrochemistry. Cyclic voltammograms (CVs) and differential pulse voltammograms (DPVs) of complexes **1**−**3** were recorded in acetonitrile with [TBA][PF_6] as supporting electrolyte in the potential range −1.2 to +0.7 V vs SCE. Typical CVs and DPVs of **1**−**3** are shown in Figure 4. The redox parameters from CVs and DPVs of **1**−**3** are essentialy identical with $E_{1/2}{}^1 = -0.57$ and $E_{1/2}{}^2 = -1.15$ V versus Fc^+/Fc, which can be ascribed to the successive redox reactions $Fe^{III}_2/Fe^{II}Fe^{III}$ and $Fe^{II}Fe^{III}/Fe_2{}^{II}$. Unfortunately, the values reported by Hendrickson and Buchanan et al. (−0.29 and −0.84 V vs Ag/AgCl[15j]) are not the correct values for complex **1**.[14] In fact,

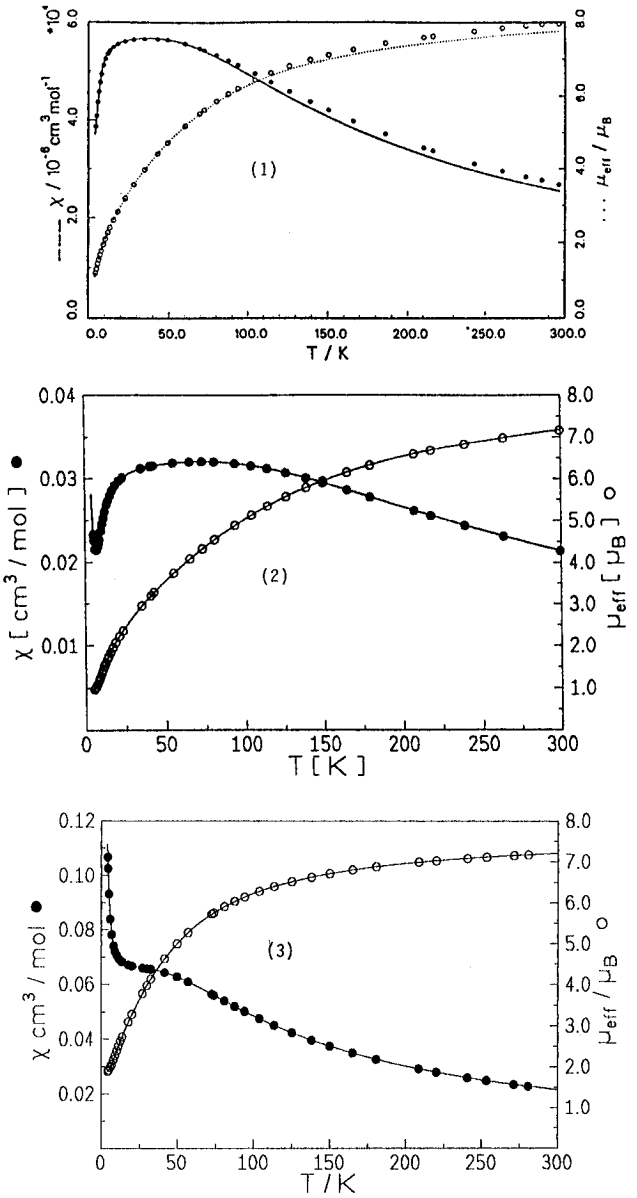

Figure 3. Magnetic susceptibility (●) and effective magnetic moment (○) of powder samples as functions of temperature for **1** (top), **2**, and **3** (bottom).

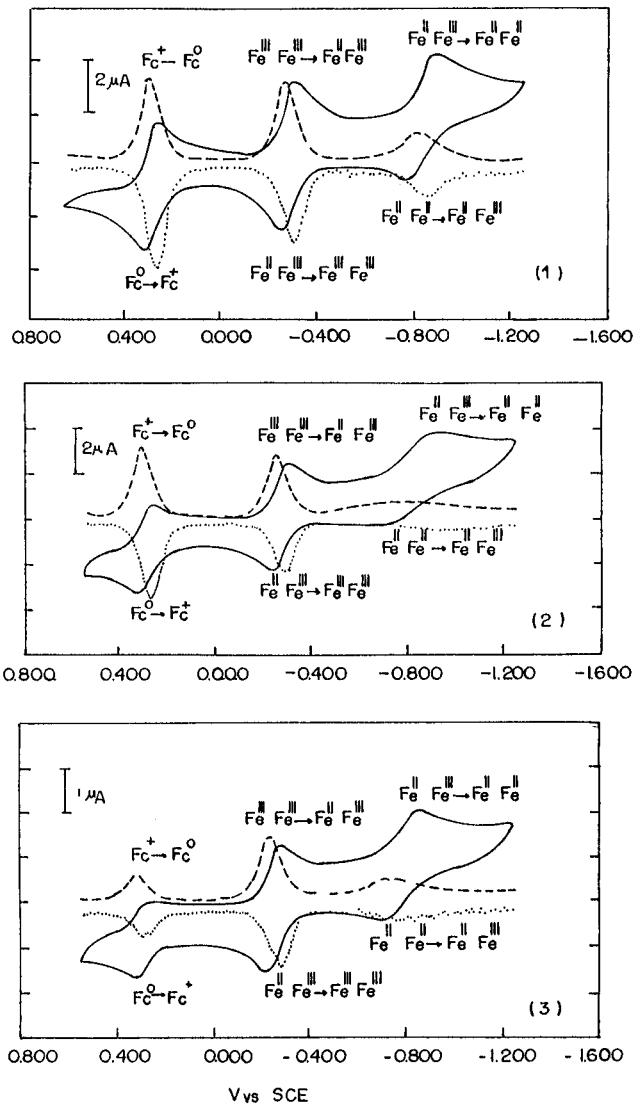

Figure 4. Cyclic voltammograms (—) and differential pulse voltammograms of **1** (top), **2**, and **3** (bottom), in CH_3CN (0.1 M [TBA][PF_6] supporting electrolyte, platinum working electrode, platinum wire auxiliary electrode, ferrocene internal standard) under argon at 100 mV/s, with two successive scans.

these redox couples (−0.04 and −0.62 V vs Ag/AgCl[24]) are shifted to more anodic potentials when compared to the reported values of −0.225 and −0.785 V vs Ag/AgCl for [Fe^{III}_2(BIOMP)(μ-OAc)$_2$]$^+$.[15j] Indeed, this reflects the relative facility of obtaining the mixed-valence complex **3** as compared to the corresponding complex with H_3BIOMP. These differences in $E_{1/2}$ values most probably arise from the distinct basic character of the 1-methylimidazole and pyridyl pendant arms in the BIOMP^{3-} and BBPMP^{3-} ligands, respectively. On the other hand, one can observe how the bridging units in the BBPMP^{3-} complexes [Fe^{III}_2(BBPMP)(μ-OAc)$_2$]$^+$, [Fe^{III}_2(BBPMP)(μ-OAc)(μ-OH)]$^+$, and [Fe^{III}_2(BBPMP)(μ-O_2P(OPh)$_2$)$_2$]$^+$ [15h] and in the BPMP$^-$ complexes [$Fe^{II}Fe^{III}$(BPMP)(μ-OAc)$_2$]$^{2+}$ and [$Fe^{II}Fe^{III}$(BPMP)(μ-OAc)(OH)]$^{2+}$ [15a] affect the reversibility of the redox processes. It is worth noting the better degree of reversibility for both redox couples of complexes **1** and **3** compared with complex **2** (Figure 4), which reflects the difference in the bridging moieties. Therefore, structural changes in solution accompaning the redox processes may be responsible for the two quasi-reversible redox couples for **1** and **2** and an irreversible reduction wave for the (μ-O_2P(OPh)$_2$)$_2$ complex of the same ligand. From the separation of the redox potentials $E_{1/2}{}^1$ and $E_{1/2}{}^2$, we have determined the stability of the mixed-valence forms of complexes **1** and **2** by evaluating their comproportionation constants ($K_{com} \cong 10^{10}$) for the equilibrium

$$[Fe^{III}_2(BBPMP)(OAc)X]^+ + [Fe^{II}_2(BBPMP)(OAc)X]^- \overset{K_{com}}{\rightleftharpoons} 2[Fe^{II}Fe^{III}(BBPMP)(OAc)X] \quad (1)$$

$$X = OAc^- \text{ for } \mathbf{1};\ X = OH^- \text{ for } \mathbf{2}$$

$$E_{1/2}{}^1 - E_{1/2}{}^2 = (RT/nF) \ln K_{com} \quad (2)$$

This value of K_{com} indicates a substantial stability of the mixed-valence complexes **3** and **4** compared with $K_{com} = 4 \times 10^6$ for the corresponding equilibrium in the [Fe^{III}_2(BBPPNOL)(μ-OAc)$_2$]$^+$ complex.[16] However, [$Fe^{II}Fe^{III}$(BBPMP)(μ-OAc)$_2$] and [$Fe^{II}Fe^{III}$(BBPMP)(μ-OAc)(μ-OH)] are approximately 2 orders of magnitude less stabilized than the well-characterized complex [$Fe^{II}Fe^{III}$(BPMP)(μ-OPr)$_2$]$^{2+}$ [15c] ($K_{com} = 7.5 \times 10^{11}$). Structural effects and Coulombic interactions are the most

(24) Gritzner, G.; Kuta, J. *Pure & Appl. Chem.* **1982**, *54*, 1527.

Table 6. Visible Absorption Properties of the Dinuclear Complexes

complex[a]	$\lambda_{max}{}^b/\epsilon^c$	ref
$[Fe^{III}_2(BBPMP)(\mu\text{-}OAc)_2]ClO_4\cdot H_2O$	≅334/7850	
	601/7700	this work
$[Fe^{III}_2(BBPMP)(\mu\text{-}OAc)(\mu\text{-}OH)]ClO_4\cdot 3H_2O$	≅334 sh	
	568/4760	this work
$[Fe^{II/III}_2(BBPMP)(\mu\text{-}OAc)_2]\cdot H_2O$	≅334 sh	
	540/4840	this work
$[Fe^{II/III}_2(BBPMP)(\mu\text{-}OAc)(\mu\text{-}OH)]$	≅334 sh	
	516/4560[d]	this work
$[Fe^{II}Fe^{III}(BPMP)(\mu\text{-}OPr)_2](BPh_4)_2\cdot CH_3COCH_3$	390 sh	
	554/950	15c

[a] In CH_3CN. [b] Units of nm. [c] Units of M^{-1} cm^{-1}/Fe_2. [d] Estimated from spectroelectrochemistry.

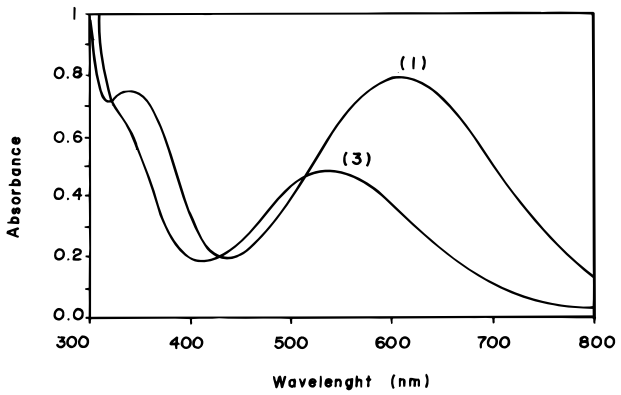

Figure 5. Visible absorption spectra of **1**, $[Fe^{III}_2(BBPMP)(\mu\text{-}OAc)_2]ClO_4\cdot H_2O$, and **3**, $[Fe^{II}Fe^{III}(BBPMP)(\mu\text{-}OAc)_2]\cdot H_2O$, in CH_3CN at room temperature.

problable factors that determine different stabilizations for **3** and **4** when compared with $[Fe^{II}Fe^{III}(BPMP)(\mu\text{-}OPr)_2]^{2+}$.

Electronic Spectroscopy and Spectroelectrochemistry. The absorption properties of the complexes in CH_3 CN are summarized in Table 6, and the visible spectra for complexes **1** and **3** are displayed in Figure 5. We have used spectroelectrochemistry to examine the electronic absorption and redox properties of $[Fe^{II}Fe^{III}(BBPMP)(\mu\text{-}OAc)_2)]$ (Figure 6a) generated in solution from complex **1**. The mantainance of isosbestic points in successive spectra strongly corroborates the presence of a single product throughout the course of the electrolyses. It is important to note that the spectrum of complex **3** (Figure 5) is identical with the spectrum of the mixed-valence species generated in solution from **1** (Figure 6a), which supports the structure proposed for **3**. The $E_{1/2}{}^1 = -0.57$ V vs Fc^+/Fc and $n = 1.0 \pm 0.1$ electron values obtained from the Nernst plot (inset in Figure 6a) are in good agreement with the CV and DPV results. Similarly, the same technique was used to generate the $[Fe^{II}Fe^{III}(BBPMP)(\mu\text{-}OAc)(\mu\text{-}OH)]$ complex in CH_3CN solution from complex **2** (Figure 6b). Interestingly, from the Nernst plot (inset in Figure 6b) we can observe a cathodic shift of 80 mV when compared to the situation of the complex with two acetate bridges, despite CV and DPV methods revealing similar redox potentials for both species. The discrepancy between the voltammetric and spectropotentiostatic data probably arises because of the instability of the fully reduced $[Fe^{II}_2(BBPMP)(\mu\text{-}OAc)(\mu\text{-}OH)]^-$ species (Figure 4) under the conditions of the voltammetric experiments. In fact, a negative shift can be expected, since hydroxide is more basic than the acetate group.

The band or shoulders at ≅334 nm are detected for complexes **1**−**4** and are assigned to phenolate-to-Fe^{III} charge transfer transitions, while the bands in the visible region appear to depend on two factors: the oxidation state of the iron centers and the nature of the bridging groups. For complexes **1** and **2**, the bands correlate well with phenolate-to-Fe^{III} CT processes; however, for the mixed-valence complexes **3** and **4**, the transitions do not seem to have the same origin as for **1** and **2**.

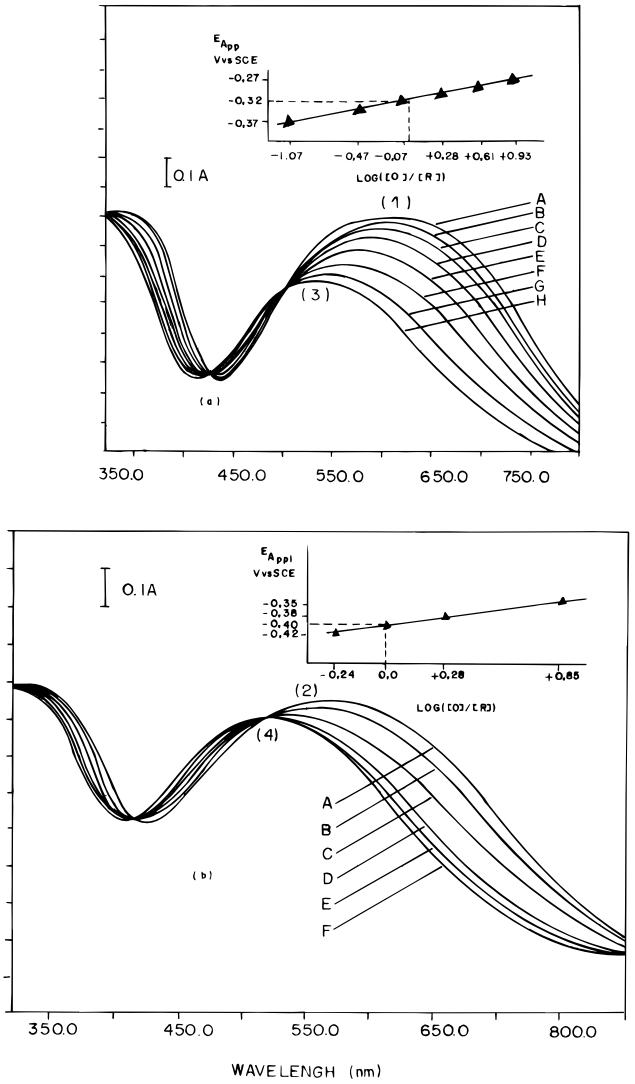

Figure 6. Spectral changes during spectropontentiostatic experiments, with time intervals between each spectrum of 90 s, for the conversion of (a) complex **1** into **3** and (b) complex **2** into **4** in CH_3CN, under argon. Applied potentials vs SCE: (a) A 0.0 V, B −0.27 V, C −0.29 V, D −0.31 V, E −0.33 V, F −0.35 V, G −0.37 V, H −0.38 V; (b) A 0.0 V, B −0.35 V, C −0.38 V, D −0.40 V, E −0.42 V, F −0.45 V.

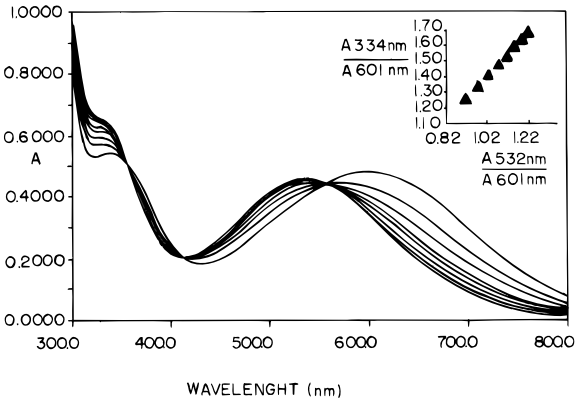

Figure 7. Spectral changes during the convertion of complex **1**, $[Fe^{III}_2(BBPMP)(\mu\text{-}OAc)_2]ClO_4\cdot H_2O$, in CH_3CN/Et_3N, into complex **2**, $[Fe^{III}_2(BBPMP)(\mu\text{-}OAc)(\mu\text{-}OH)]ClO_4$, with time intervals of 150 s.

On the basis of the ϵ values and the hypsocromic shifts observed for **3** and **4**, we tentatively assigned them as phenolate-to-Fe^{III} combined with Fe^{II} -to-pyridine CT transitions.[16] A similar assignment has been used for the mixed-valence complex $[Fe^{II}Fe^{III}(BPMP)(\mu\text{-}OPr)_2]^{2+}$,[15c] where the Fe^{II}-to-pyridine band is shifted to higher energy as compared to the phenolate-to-Fe^{III}

Scheme 1. Proposed Reactions among **1**−**4**

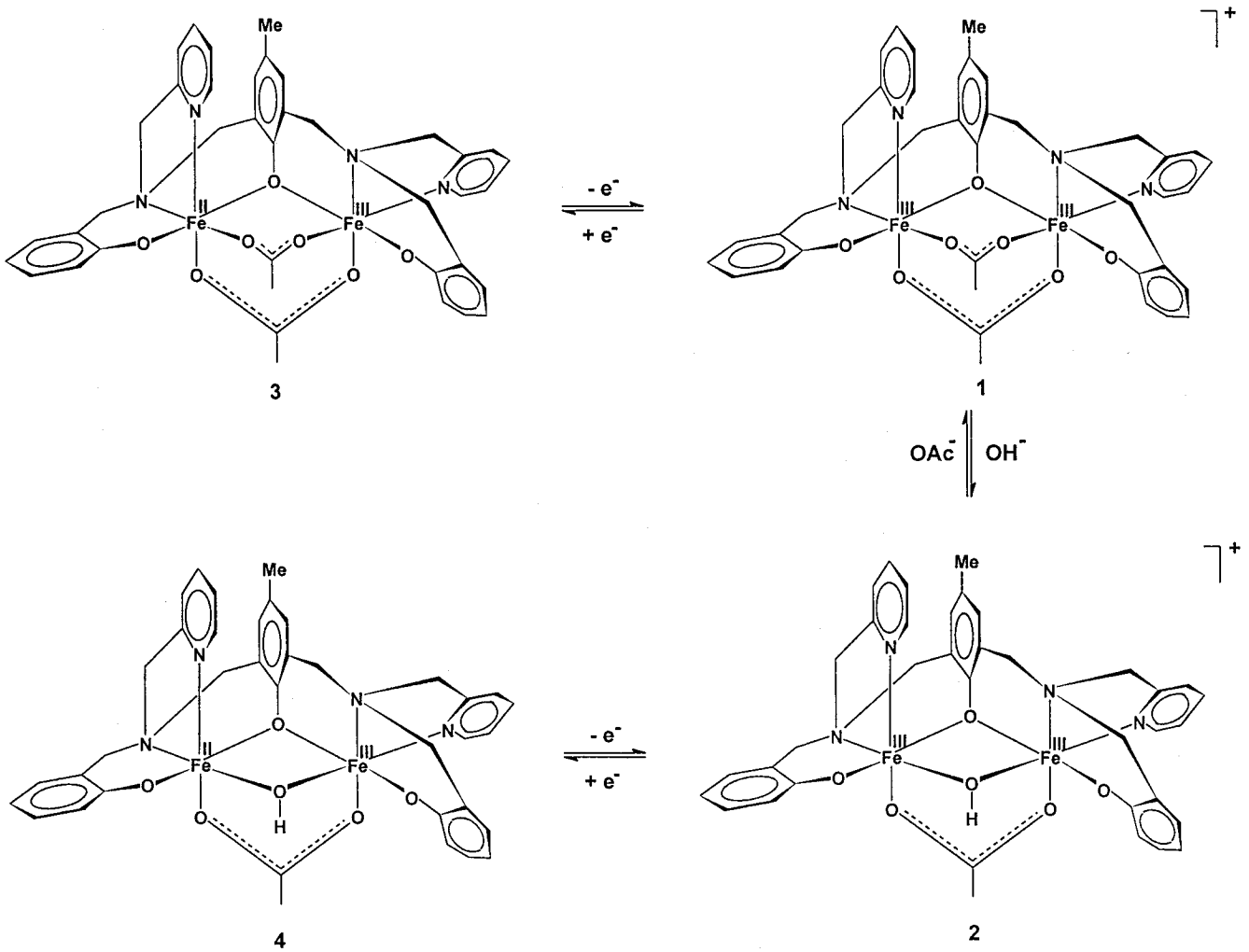

band. Interestingly, neither **3** nor **4** has shown intervalence transfer absorption bands, in CH_3CN, in the near-IR region. However, from the compropotionation constant value ($K_{com} \cong 10^{10}$), which suggests a great deal of stabilization in the ground state,[25] we tentatively assigned both complexes as type II mixed-valence species in the Robin and Day classification.[26] Finally, $[Fe^{III}_2(BBPMP)(\mu\text{-}OAc)(\mu\text{-}OH)]^+$, $\lambda_{max} = 568$ nm/$\epsilon = 4.760$ M^{-1} cm^{-1}, and $[Fe^{II}Fe^{III}(BBPMP)(\mu\text{-}OAc)(\mu\text{-}OH)]$, $\lambda_{max} = 516$ nm/$\epsilon = 4.560$ M^{-1} cm^{-1}, are good synthetic analogues of the chromophoric site for the oxidized and reduced forms of PAPs.

As described in the Experimental Section, complex **2** was obtained from complex **1** in $CH_3CN/H_2O/KOH$. The reaction was followed spectrophotometrically, and as illustrated in Figure 7, $[Fe^{III}_2(BBPMP)(\mu\text{-}OAc)_2]^+$ is cleanly converted to $[Fe^{III}_2(BBPMP)(\mu\text{-}OAc)(\mu\text{-}OH)]^+$. A linear plot (inset in Figure 7) indicates[27] two species in solution with no restrictions on stoichiometry. The reaction of $[Fe^{III}_2(BBPMP)(\mu\text{-}OAc)(\mu\text{-}OH)]^+$ in $CH_3CN/H_2O/CH_3COOH$ was also followed and showed the same isosbestic points, back to the spectrum of $[Fe^{III}_2(BBPMP)(\mu\text{-}OAc)_2]^+$. Unfortunately, we were not able to obtain suitable crystals of neither **2** nor **3** for X-ray analyses. However, considering the properties of these complexes and the structure of the cations of **1**, we propose Scheme 1 to correlate the model complexes.

Summary and Perspectives. We have synthesized and characterized Fe^{III}_2 and $Fe^{II}Fe^{III}$ complexes of the dinucleating ligand H_3BBPMP, as analogues for the active site of PAPs. The complexes exhibit novel IR, Mössbauer, magnetic, electrochemical, and electronic absorption properties that improve the understanding of the oxidized and reduced forms of the enzymes. The complexes $[Fe^{III}_2(BBPMP)(\mu\text{-}OAc)_2]^+$ and $[Fe^{III}_2(BBPMP)(\mu\text{-}OAc)(\mu\text{-}OH)]^+$ can be interconverted in solution, and the processes illustrated how to adjust the chromophore in order to have a model for the active site of the proteins. However, due to the presence of two terminal phenolate groups, the redox couples lie at more negative potentials than those detected for PAPs.[17] In order to mimic the electrochemical properties for the $Fe^{III}_2/Fe^{II}Fe^{III}$ redox potential reported for PAPs,[17] we recently prepared a new unsymmetrical N_5O_2−donor dinucleating ligand, 2-[((2-pyridylmethyl)amino)methyl]-6-[((2-hydroxybenzyl)(2-pyridylmethyl)amino)methyl]-4-methylphenol ($H_2BPBPMP$) and its first $Fe^{II}Fe^{III}$ complex as a model for the redox properties of uteroferrin.[28] The syntheses of new dinuclear complexes of iron, vanadium, manganese, nickel, copper, and zinc, including heterobimetallic species, with H_3BBPMP and $H_2BPBPMP$ are in progress in our laboratory and will be the subject of future reports.

Acknowledgment. This work was supported by grants from the CNPq, PADCT, and FINEP (Brazil) and KFA (Germany).

Supporting Information Available: Tables giving all bond distances and angles, anisotropic temperature factors, and hydrogen atom coordinates (13 pages). Ordering information is given on any current masthead page.

IC950456V

(25) Creutz, C. *Prog. Inorg. Chem.* **1983**, *30*, 1.
(26) Robin, M. B.; Day, P. *Inorg. Chem. Radiochem.* **1967**, *10*, 247.
(27) Coleman, J. S.; Varga, L. P.; Mastin, S. H. *Inorg. Chem.* **1970**, *9*, 1015.
(28) Neves, A.; de Brito, M. A.; Drago, W.; Griesar, K.; Haase, W. *Inorg. Chim. Acta* **1995**, *237*, 131.